Journal of Alloys and Compounds 511 (2012) 202–208

Contents lists available at SciVerse ScienceDirect

Journal of Alloys and Compounds

journal homepage: www.elsevier.com/locate/jallcom

Controlled synthesis of TiO_2 mesoporous microspheres via chemical vapor deposition

Junwei Hou [a], Xiuchun Yang [a,*], Xiaoyi Lv [b], Min Huang [a], Qingyao Wang [a], Jun Wang [c]

[a] School of Material Science and Engineering, Tongji University, Shanghai 200092, PR China
[b] Postdoctoral Station of Computer Science and Technology, Xinjiang University, Urumqi 830046, China
[c] Ningbo Institute of Material Technology and Engineering, Chinese Academy of Sciences, Ningbo 315201, PR China

ARTICLE INFO

Article history:
Received 1 August 2011
Received in revised form
12 September 2011
Accepted 13 September 2011
Available online 19 September 2011

Keywords:
Mesoporous
Chemical vapor deposition
TiO_2
Ostwald ripening

ABSTRACT

Anatase titanium dioxide (TiO_2) mesoporous microspheres with core–shell and hollow structure were successfully prepared on a large scale by a one-step template-free chemical vapor deposition method. The effects of various reaction conditions on the morphology, composition and structure of the products were investigated by scanning electron microscopy (SEM), transmission electron microscopy (TEM), X-ray diffraction (XRD), X-ray photoelectron spectroscopy (XPS), Brunauer–Emmett–Teller (BET) technique and photoluminescence (PL) method. The results indicate that the product near the source was composed of core–shell structure TiO_2 microspheres with diameters from 3 to 5 μm. With increasing the distance between the source materials and the substrate, the hollow TiO_2 spheres with 1–2 μm dominant the products. A localized Ostwald ripening can be use to explain the formation of core–shell and hollow structures, and the size of the initial TiO_2 solid nanoparticles plays an important role in determining the evacuation manner of the solid in the ripening-induced hollowing process. The surface area of TiO_2 hollow microspheres determined by the adsorption isotherms was measured to be 74.67 m^2/g. X-ray photoelectron spectroscopy (XPS) analysis revealed that the O–H peaks of hollow structures have a chemical shift compared with the core–shell structures. The optical property of the products was also discussed.

1. Introduction

Recently, hollow structures with a unique size distribution and well-defined morphology are of particular interest because of their interesting properties and potential applications in optical [1], electronic [2], biological [3,4], and magnetic [5] fields. Many hollow spheres such as ZnS [6], $BaTiO_3$ [7], Cu_2O [8], and SiO_2 [9], have been prepared. As one kind of important semiconductor material, anatase phase TiO_2 is a better choice to use as photocatalysts [10–13], gas sensors [14], surface functionalization [15], biomaterials [16], lithium batteries [17] and solar cells [18,19] due to its nontoxicity, low cost, and delivering ability. Many methods have been reported to synthesize TiO_2 mesoporous structures in the literature [20–22]. Li and co-workers [23] described a sol-spraying-calcination method to fabricate a new type of TiO_2 microsphere photocatalyst with a particle size of 30–160 nm. Xie and co-workers [24] reported the fabrication of crystallized rutile phase TiO_2 hollow spheres by a simple hydrothermal method using potassium titanium oxalate as the precursor. More recently, Chen and co-workers [25] fabricated long TiO_2 hollow fibers with mesoporous walls, which showed high photo-catalytic activity, by means of a sol–gel process combined with a two-capillary spinneret electrospinning technique. Yang et al. [26] reported the synthesis of anatase TiO_2 microspheres via Ostwald ripening after a long hydrothermal treatment. Dong et al. [27] prepared mesoporous spheres of metal oxides on the basis of the two-step nanocasting route. Ren et al. [28] have prepared hollow microspheres of mesoporous TiO_2 adopting the surfactant-assisted method. However, most of the existing methods use intrinsically costly precursors, templates, and high temperature procedure, the development of cost-effective methods suitable for the large-scale synthesis of TiO_2 nanostructure materials is still a challenge.

In this letter, we presented a facile chemical vapor deposition technology to synthesize core–shell and hollow anatase TiO_2 microspheres with a large surface area. The products were formed by the self-organization of a large number of small grains. The morphology evolution and formation mechanism were also investigated. The BET results showed that these nanostructures were with high surface area. These nanostructures can be used as promising

* Corresponding author. Tel.: +86 21 69580446.
E-mail address: yangxc@tongji.edu.cn (X. Yang).

0925-8388/$ – see front matter © 2011 Elsevier B.V. All rights reserved.
doi:10.1016/j.jallcom.2011.09.032

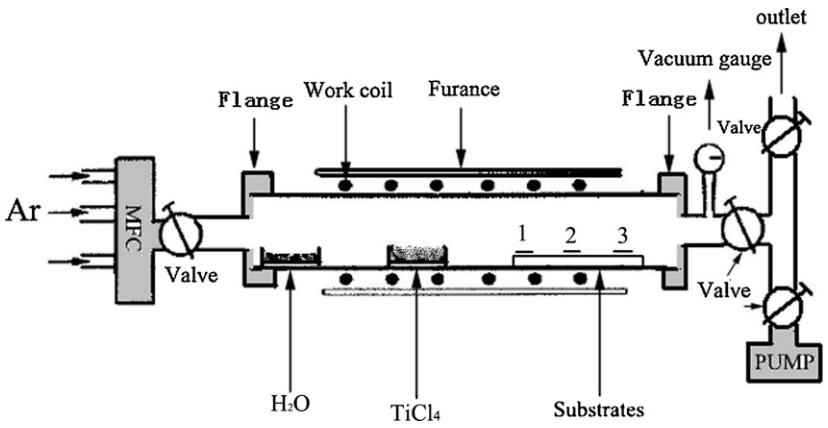

Fig. 1. Schematic illustration of the furnace used in the experiment.

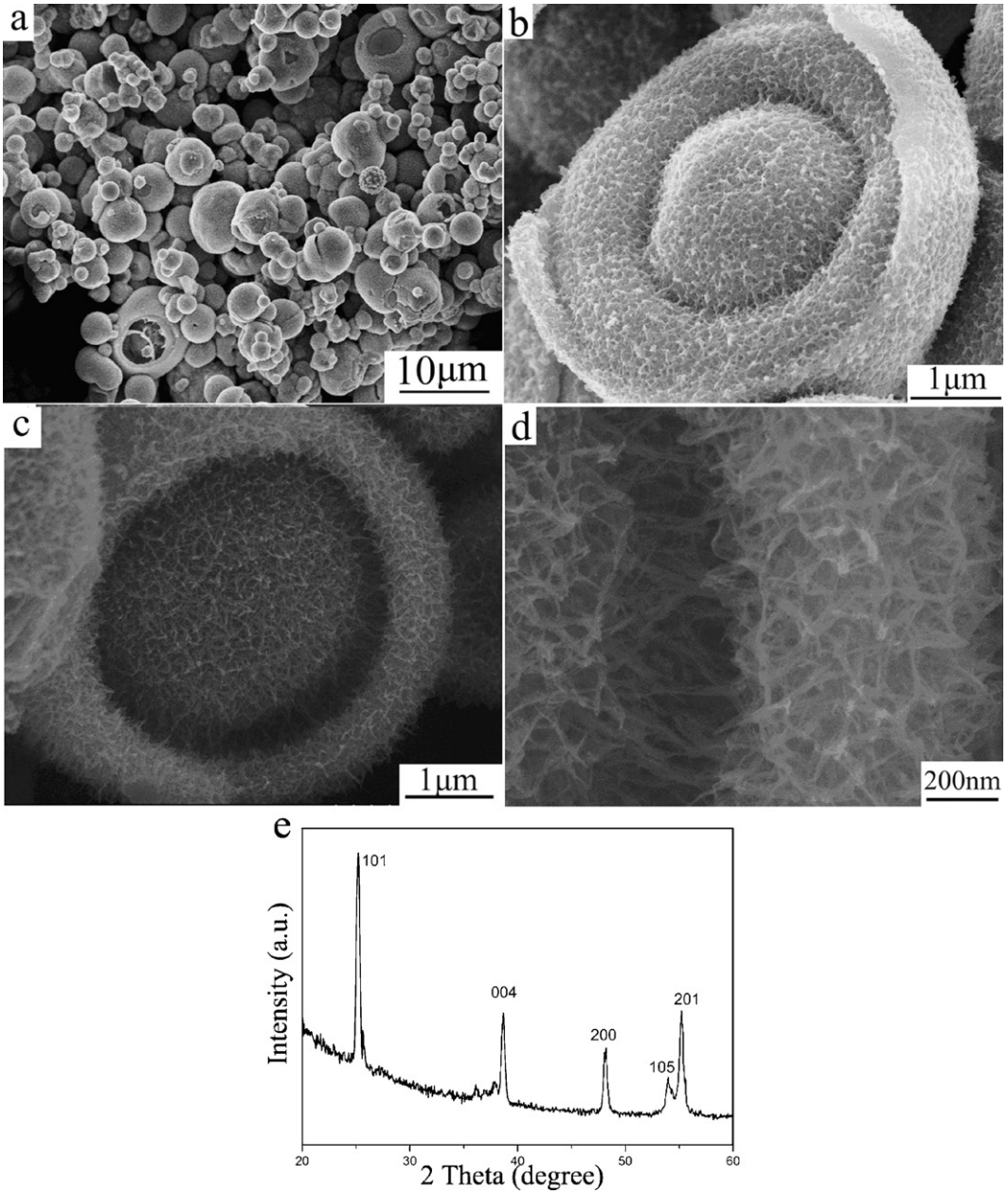

Fig. 2. SEM images with different magnifications (a–d) and XRD pattern (e) of the sample 1 on substrate 1 for 1 h.

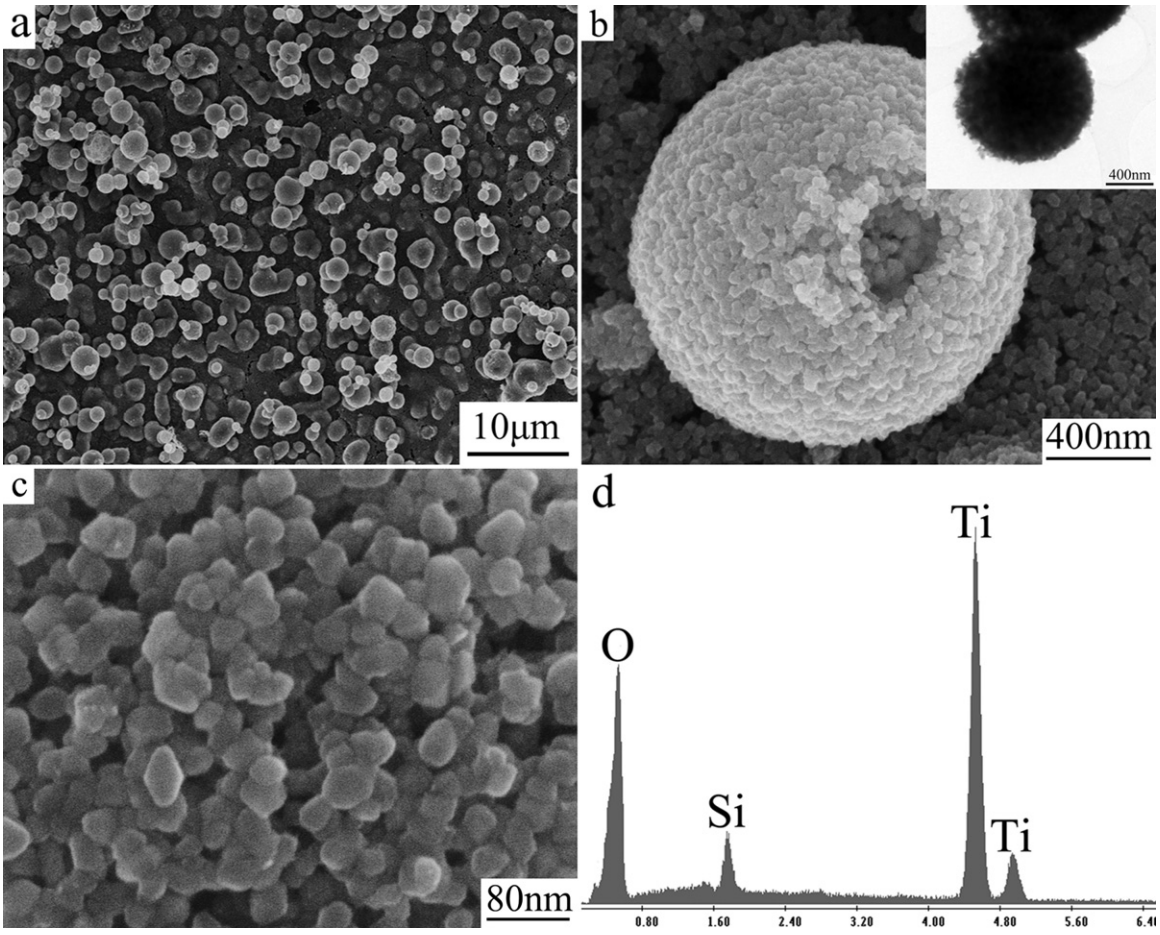

Fig. 3. SEM images with different magnifications (a–c) and EDS pattern (d) of the sample 2 on substrate 2 for 1 h.

supporting materials in a variety of applications such as solar cells, biosensors, catalysts, etc.

2. Experimental

The CVD apparatus for sample fabrication is illustrated in Fig. 1.

De-ionized water, as the oxide source, was placed in front of the horizontal alumina tube, and $TiCl_4$ (Aldrich 99.9%) was placed in the heating center as the titanium source. Three pieces of silicon (1 0 0) substrates were placed downstream in the horizontal alumina tube for materials growth. The distance between the first silicon substrate (sample 1) and the $TiCl_4$ source is 12 cm, and the distance between two neighboring substrates is 3 cm as shown in Fig. 1. Prior to heating, the system was evacuated and flushed with high pure Ar atmosphere for 1 h to eliminate oxygen. Then the furnace was heated to 600 °C in 90 min and held at the temperature for 60 min under a constant Ar flow rate of 50 SCCM (standard cubic centimeters/minute), and subsequently cooled to room temperature naturally. White products could be observed on the surface of different silicon substrates.

A Mac science X-ray diffractometer (XRD) with Cu Kα radiation was used to characterize phase composites of the samples. A Philips XL 30 FEG scanning electron microscope (SEM) with an energy-dispersive X-ray spectroscope (EDS) was used to observe the morphologies and elemental compositions of the samples. A JEOL 2010 transmission electron microscope (TEM) with selected-area electron diffraction (SAED) was used to analyze the morphology and microstructure. A JEOL JPS90SX photoelectron spectrometer with an Mg Kα source (1253.6 eV) was

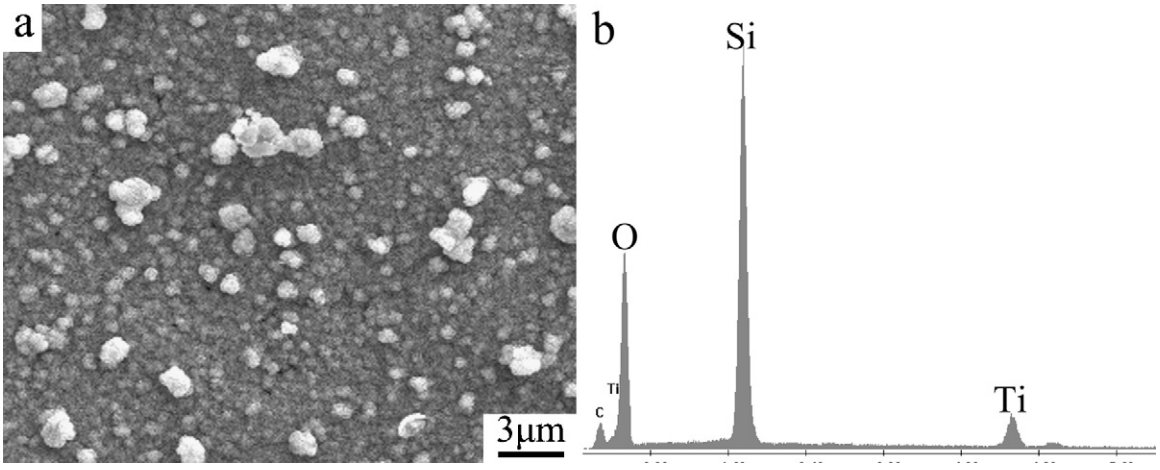

Fig. 4. SEM image (a) and EDS pattern (b) of the sample 3 on substrate 3 for 1 h.

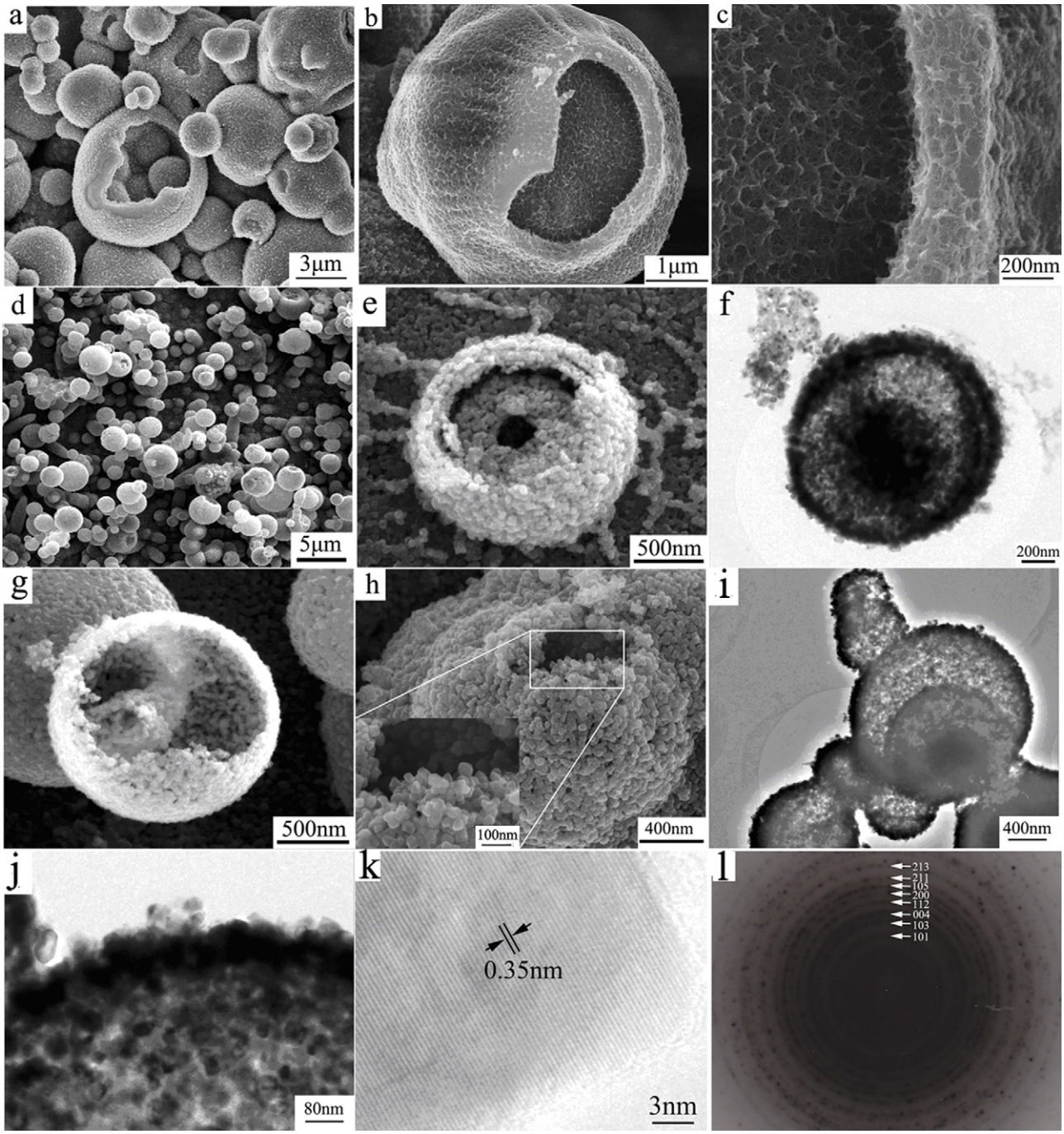

Fig. 5. SEM (a–c) images of the sample 4 on substrate 1 for 5 h; SEM (d and e) and TEM (f) images of the sample 5 on substrate 2 for 5 h; SEM (g and h), TEM (i and j), HRTEM (k) images and SAED pattern (l) of the sample 6 on substrate 2 for 10 h. The inset in (h) is the high magnification image of region which marked with a white rectangle in (h).

used to measure the X-ray photoelectron spectra (XPS). The pore-size distribution of the hollow structure and the nanocrystalline electrode was obtained by Brunauer–Emmett–Teller (BET) measurements (Bel Japan, Belsorpmax) (Nitrogen, 77 K). Room temperature photoluminescence spectrum (PL) was carried out with a Hitachi F-7000FL spectrophotometer.

3. Result and discussion

Fig. 2 gives SEM images of sample 1.

Fig. 2a shows a low-magnification SEM image of the as-grown sample deposited on substrate 1 for 1 h, which indicates that the products are composed of a large number of microspheres with diameters of about 2–5 μm. The core–shell architecture is readily apparent from SEM images of broken spheres (Fig. 2b). The high magnification SEM image (Fig. 2c and d) clearly reveals that the mesoporous microspheres are constructed by numerous irregular nanorods with a length ranging from 150 to 200 nm. The bird nest-like structure has many interstitial spaces, which could provide connected channels for mass exchange between the inner space of TiO_2 microspheres and the outer solution. The XRD peaks in Fig. 2e could be assigned as (1 0 1), (0 0 4), (2 0 0), (1 0 5) and (2 0 1) lattice surfaces of anatase TiO_2 (JCPDS No.21-1272), indicating that sample 1 is composed of highly crystallized anatase TiO_2. These results indicate that anatase-phase TiO_2 hollow microspheres have been successfully synthesized on a large scale.

Fig. 3 gives SEM images of sample 2.

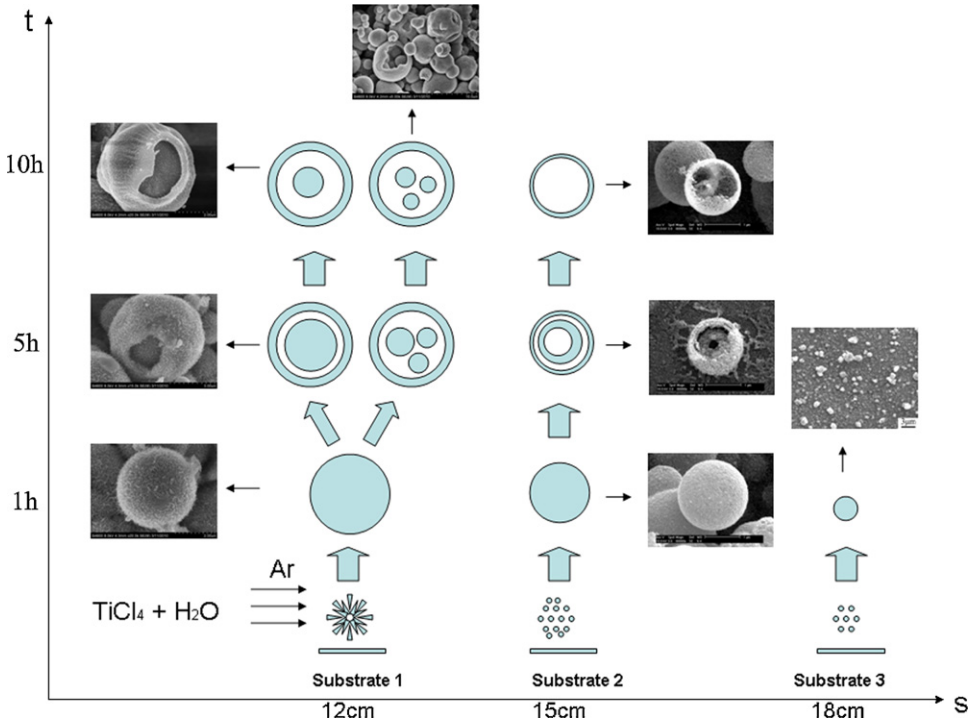

Fig. 6. Illustration for formation mechanisms of core–shell and hollow structures.

Fig. 3a indicates that sample 2 is composed of numerous microspheres with diameters of 1–2 μm, which is smaller than the microsphere size in sample 1. The high magnification SEM images as shown in Figs. 3b and c reveal that the TiO_2 microspheres are made up of nanoparticles with size of about 40 nm. The EDX pattern in Fig. 3d shows that the micro-spheres are composed of pure TiO_2. The trace amount of Si is from the silicon substrates.

Fig. 4 gives SEM images of sample 3.

The SEM image of the sample deposited on substrate 3 is shown in Fig. 4. Only little TiO_2 particles are observed on the substrate 3. The EDS shows that only the peaks for titanium, silicon and oxygen are observed, and the peak of Si is higher than those of Ti and O, confirming that the concentration of TiO_2 decreases rapidly.

Fig. 5 gives SEM and TEM images of the as-prepared samples with different reaction conditions.

In order to reveal the formation mechanism of hollow TiO_2 spheres, time-dependent reactions were carried out to investigate the growth process in detail and distinct evolution stages were obtained. Fig. 5a–c show the morphology of the sample 4 obtained on substrate 1 for 5 h. Compared with the sample 1, it is found that the core of sphere shrinks and the inner space is increased continually. A multi core–shell structure can be observed from one broken sphere. Fig. 5d–f show the morphology of the sample 5 obtained on substrate 2 for 5 h. It can be seen that the core is entirely detached from the shell, and formed a unique core–shell structure. The core finally diminished after 10 h reaction time and a hollow structure appeared on sample 6. The morphologies and microstructures of sample 6 were further investigated by SEM (Fig. 5g and h), TEM (Fig. 5i and j), HRTEM (Fig. 5k), and SAED (Fig. 5l). The inset of Fig. 5h gives a magnified SEM image of one broken sphere with a hole in the shell, indicating clearly its hollow structure. The diameters of these hollow spheres are approximately 1–2 μm, and the rough surface of each shell indicates that it is assembled by nano-grains. SAED pattern indicates that the diffraction rings of the anatase phase TiO_2 (1 0 1), (1 0 3), (0 0 4), (1 1 2), (2 0 0), and (1 0 5) reflections. HRTEM image shows the lattices spacing between the adjacent planes is 0.35 nm, corresponding to (1 0 1) plane of anatase-phase TiO_2.

Fig. 6 gives schematic illustration of the formation process of TiO_2 core–shell and hollow nanostructures.

It is interesting to understand the formation mechanism of the TiO_2 core–shell and hollow structures since no hard or soft templates were used in the synthesized process. Local Ostwald ripening [29] is believed to be responsible for the hollow structure, and the formation processes are illustrated in Fig. 6. At the initial stage, the amorphous TiO_2 nanocrystals are formed by hydrolyzation of $TiCl_4$. With continuous nucleation and growth of TiO_2, larger TiO_2 solid spheres would form due to the aggregation of primary crystallites. Further evacuation of the TiO_2 particles takes place with prolonging reaction time. The surface layer of the spheres crystallizes first generate due to contraction with the surrounding solution. As a result, the materials inside the solid spheres have a strong tendency to dissolve, which provides the driving force for the spontaneous inside-out Ostwald ripening. This dissolution process could initiate at regions around the ripening center of the solid spheres, in which the nanoparticles have highest surface energies. For the small homogeneous spheres, the hollow single core/shell particles were formatted at last because the ripening center of small homogeneous spheres usually were coincident with the geometric center. For some bigger non-homogeneous spheres, several ripening centers appear simultaneously, to produce multi core–shell particles [37].

The size of the initial solid nanoparticles also plays an important role in determining the hollowing process. When the initial particles have a larger size, it is very difficult for the solid evacuation to initiate at regions around the center of the solid particles, because the thick shell would inhibit the outward diffusion of the dissolved species. And thus the solid evacuation can only start underneath the surface layer of the particles, which results in the formation of the core–shell structures. On the contrary, smaller initial particles would favor the solid evacuation from the center region, and only hollow products come into being in the ripening process. In our study, near the source materials, the TiO_2 concentration are very high, the initial solid nanorods have a size in the range of 150–200 nm, so the single and multi core–shell TiO_2 spheres

Table 1
The BET surface area and total pores volume for different samples.

Samples	Surface area ($m^2\ g^{-1}$)	Pore volume ($cm^3\ g^{-1}$)
TiO_2 hollow sphere (samples 6)	74.67	0.22
TiO_2 core–shell sphere (sample 4)	39.22	0.15

finally become the dominant products. With the increase in distance between the source materials and the substrate, the TiO_2 concentration decrease rapidly so the initial TiO_2 gains have an average size of about 30–40 nm on substrate 2, and thus hollow TiO_2 spheres appear in the products.

Table 1 gives the BET surface area and total pores volume for different samples.

Fig. 7 gives BET results of the sample 6.

The BET surface area values for different samples are given in Table 1. Compared with sample 4, it can be observed that the higher values of the surface area and total pore volume were obtained for the sample 6. The Nitrogen adsorption–desorption isotherms and the Barrett–Joyner–Halenda (BJH) pore size distribution plots of the sample 6 are shown in Fig. 7a and b, respectively. These products were found to be mesoporous with mean pore diameter of 91.0–102.3 nm, which can be attributed to the interstitial voids resulting from the relatively loose packing of the nanocrystallites. Such mesoporous titanium dioxide have been found to exhibit high photocatalytic activity and hence can potentially be used in biomemitic photocatalysis and dye-sensitized solar cells [30,31].

Fig. 8 gives XPS results of the as-prepared core–shell and hollow structure.

Quantitative XPS analysis was performed on the core-shell (sample 4) and hollow (sample 6) titanium dioxide spheres. The high-resolution XPS spectra of O1s are reported in Fig. 8a and b. The Lorentzian/Gaussian mix values were used in the curve resolution of the individual O1s peaks in the two spectra. For the core–shell structure, the O1s region is decomposed into two contributions. The main contribution is attributed to Ti–O (529.9 eV) in TiO_2, and the other oxygen contributions can be ascribed to the O–H (531.5 eV) in Ti–OH [32,33], respectively. For the hollow structures, the O1s region is decomposed into three contributions: the Ti–O (529.9 eV) in TiO_2, the O–H (532 eV) in Ti–OH and the Si–O (532.5 eV) [32], respectively. Compared with core shell structure, the O–H peaks of hollow structures have a chemical shift from 531.5 eV to 532 eV, this is probably due to the fact that the hollow structures easily adsorb water vapor from air, leading to the formation of hydroxyl. The Si–O in the hollow structure appears significantly when the deposition time is over 5 h, which is caused by the diffusion of Si element from the surface of substrate into the TiO_2 hollow spheres [33].

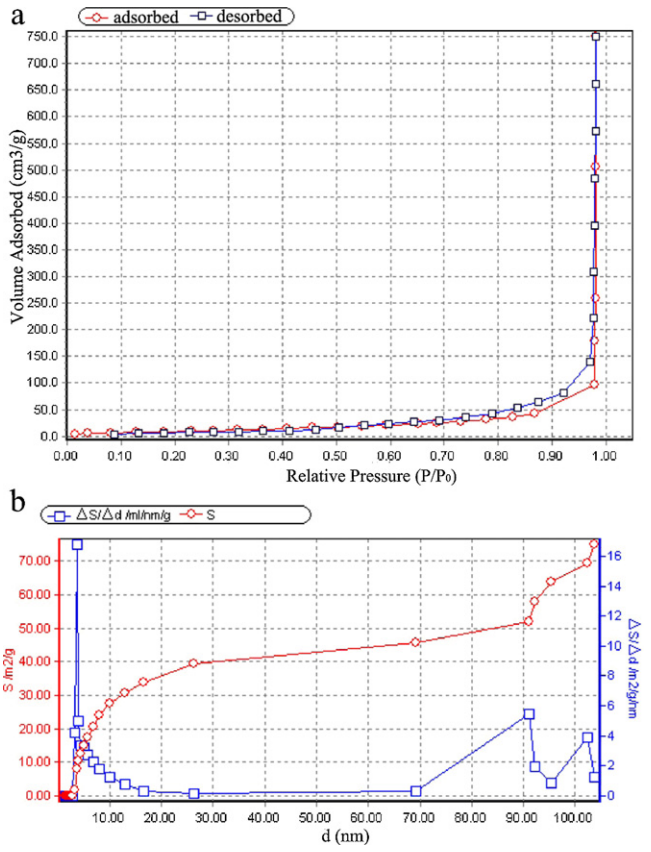

Fig. 7. N_2 adsorption and desorption isotherm of TiO_2 hollow spheres (a), and pore-size distribution curve (b) of hollow microspheres.

Fig. 9 gives PL spectrums of the as-prepared core–shell and hollow structure.

Fig. 9 shows the room temperature photoluminescence spectra for TiO_2 core–shell (sample 4) and hollow structures (sample 6), respectively. The emission peak appears at about 473 nm wavelength, which is originated from the charge-transfer transition from Ti^{3+} to oxygen anion in a TiO_6^{8-} complex [34]. The difference of about 0.6 eV between the band gap energy (3.2 eV for anatase) and the emission peak energy (2.6 eV) is

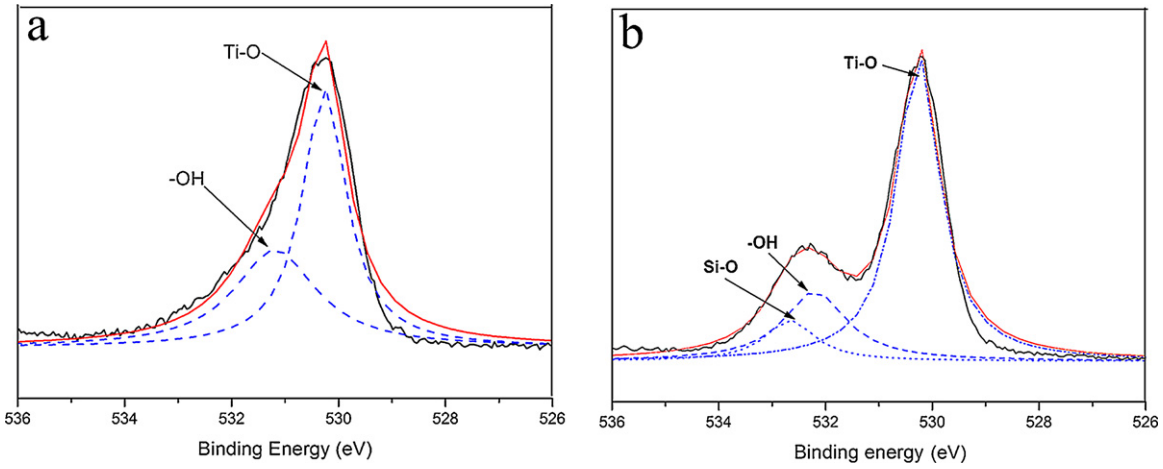

Fig. 8. X-ray photoelectron spectroscopy core-level analyses: (a) the O1s spectra of TiO_2 core–shell (sample 4) and (b) hollow structures (sample 6).

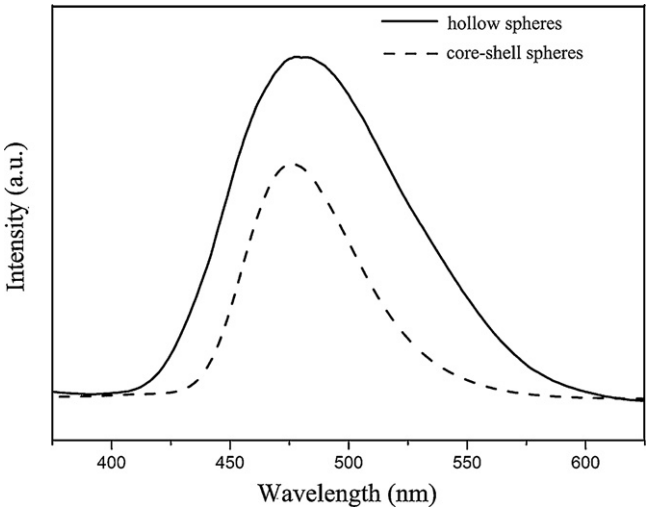

Fig. 9. The room-temperature photoluminescence spectra of TiO_2 core–shell (sample 4) and hollow structures (sample 6).

caused by the Stokes shift due to the Franck Condon effect [35–37]. In addition, the PL emission intensity mainly results from the recombination of excited electrons and holes [38], and the recombination rate is determined by the reaction temperature. The higher the reaction temperature is, the lower the PL intensity is [39]. For sample 4, near the source materials, the reaction temperature is high, so the lower PL intensity was observed.

4. Conclusion

In summary, we have successfully synthesized anatase TiO_2 core–shell and hollow structures using $TiCl_4$ and water as the precursors. A template-free chemical vapor deposition strategy is designed to construct the mesoporous nanostructure. The morphology evolution process as well as formation mechanism were also elucidated. The size of the initial solid nanoparticles played an important role in determining the evolution manner in the ripening-induced hollowing process, and an elevated deposition time was a prerequisite to initiate the hollowing evolution. This simple, general, clean, and convenient method presented here could provide a novel pathway to the synthesis of hollow spheres with complicated structure, and offer a new material platform for catalyst, microelectronic, and other applications.

Acknowledgements

This work has been supported by Key Item for Basic Research of Shanghai (No. 05JC14058) and the National Natural Science Foundation of China (No. 50672069).

References

[1] E.M. Chan, R.A. Mathies, A.P. Alivisatos, Nano Lett. 3 (2003) 199.
[2] X. Wang, J. Zhuang, Q. Peng, Y.D. Li, Nature 437 (2005) 121.
[3] X.Y. Kong, Z.L. Wang, Nano Lett. 3 (2003) 1625.
[4] T. Nakashima, N.J. Kimizuka, J. Am. Chem. Soc. 125 (2003) 6386.
[5] J. Goldberger, R. He, Y. Zhang, S. Lee, H. Yan, H.J. Choi, P. Yang, Nature 422 (2003) 599.
[6] K.P. Velikov, A.V. Blaaderen, Langmuir 17 (2001) 4779.
[7] X.L. Tian, J. Li, K. Chen, J. Han, S.L. Pan, Y.J. Wang, X.Y. Fan, F. Li, Z.X. Zhou, Cryst. Growth Des. 10 (2010) 3990.
[8] C.C. Huang, J.R. Hwu, W.C. Su, D.B. Shieh, Y. Tzeng, C.S. Yeh, Chem. Eur. J. 12 (2006) 3805.
[9] K.H. Rhodes, S.A. Davis, F. Caruso, B.J. Zhang, S. Mann, Chem. Mater. 12 (2000) 2832.
[10] X.G. Han, Q. Kuang, M.S. Jin, Z.X. Xie, L.S. Zheng, J. Am. Chem. Soc. 131 (2009) 3152.
[11] G.K. Mor, M. Shankar, M. Paulose, O.K. Varghese, C.A. Grimes, Nano Lett. 6 (2006) 215.
[12] H.G. Kim, D.W. Hwang, J.S. Lee, J. Am. Chem. Soc. 126 (2004) 8912.
[13] Q. Xiao, Z.C. Si, Z.M. Yu, G.Z. Qiu, J. Alloys Compd. 450 (2008) 426.
[14] Y. Zhu, J. Shi, C. Zhang, X. Zhang, Anal. Chem. 74 (2002) 120.
[15] A. Fujishima, K. Honda, Nature 238 (1972) 37.
[16] F. Caruso, R.A. Caruso, H. Mohwald, Science 282 (1998) 1111.
[17] L. Aldon, P. Kubiak, A. Picard, J.C. Jumas, F. Olivier, J. Chem. Mater. 18 (2006) 1401.
[18] Y. Itzhaik, O. Niitsoo, M. Page, G. Hodes, J. Phys. Chem. C 113 (2009) 4254.
[19] K. Shankar, J. Bandara, M. Paulose, H. Wietasch, O.K. Varghese, G.K. Mor, T.J. LaTempa, M. Thelakkat, C.A. Grimes, Nano Lett. 8 (2008) 1654.
[20] J. Zheng, Z.Q. Liu, X. Liu, X. Yan, D.D. Li, W. Chu, J. Alloys Compd. 509 (2011) 3771.
[21] K.S. Das, M.K. Bhunia, A. Bhaumik, Dalton Trans. 39 (2010) 4382.
[22] A.K. Patra, S.K. Das, A. Bhaumik, J. Mater. Chem. 21 (2011) 3925.
[23] X.Z. Li, H. Liu, L.F. Cheng, H.J. Tong, Environ. Sci. Technol. 37 (2003) 3989.
[24] X.X. Li, Y.J. Xiong, Z.Q. Li, Y. Xie, Inorg. Chem. 45 (2006) 3493.
[25] S.H. Zhan, D.R. Chen, X.L. Jiao, C.H. Tao, J. Phys. Chem. B 110 (2006) 11199.
[26] H.G. Yang, H.C. Zeng, J. Phys. Chem. B 108 (2004) 3492.
[27] A.G. Dong, N. Ren, Y. Tang, Y.J. Wang, Y.H. Zhang, W.M. Hua, Z. Gao, J. Am. Chem. Soc. 125 (2003) 4976.
[28] T.Z. Ren, Z.Y. Yuan, B.L. Su, Chem. Phys. Lett. 374 (2003) 170.
[29] W.Z. Ostwald, Phys. Chem. 34 (1900) 495.
[30] J. Yu, Y. Su, B. Cheng, Adv. Funct. Mater. 17 (2007) 1984.
[31] Y.J. Kim, M.H. Lee, H.J. Kim, G. Lim, Y.S. Choi, N.G. Park, K. Kim, W.I. Lee, Adv. Mater. 21 (2009) 3668.
[32] B. Erdem, R.A. Hunsicker, G.W. Simmons, E.D. Sudol, V.L. Dimonie, M. El-Aasser, Langmuir 17 (2001) 2664.
[33] R.L. Kurtz, R. Stockbauer, T.E. Madey, Surf. Sci. 218 (1989) 178.
[34] J.C. Yu, J.G. Yu, W.K. Ho, L.Z. Zhang, Chem. Mater. 14 (2002) 3808.
[35] K. Fujihara, S. Izumi, T. Ohno, M.J. Matsumura, Photochem. Photobiol. A 132 (2000) 99.
[36] N. Serpone, D. Lawless, R. Khairutdinov, J. Phys. Chem. 99 (1995) 16646.
[37] X.W. Lou, L.A. Archer, Z.C. Yang, Adv. Mater. 20 (2008) 3987.
[38] X.Z. Li, F.B. Li, C.L. Yang, W.K. Ge, J. Photochem. Photobiol. A 141 (2001) 209.
[39] J.G. Yu, H.G. Yu, B. Cheng, X.J. Zhao, J.C. Yu, W.K. Ho, J. Phys. Chem. B 107 (2003) 13871.